JAAS

View Online
Dynamic Article Links

Cite this: DOI: 10.1039/c1ja10204d

www.rsc.org/jaas

PAPER

Evaluation of manganese-bodies removal in historical stained glass windows *via* SR-μ-XANES/XRF and SR-μ-CT†

Simone Cagno,*[a] Gert Nuyts,[a] Simone Bugani,[b] Kristel De Vis,[c] Olivier Schalm,[c] Joost Caen,[c] Lukas Helfen,[d] Marine Cotte,[e] Peter Reischig[d] and Koen Janssens[a]

Received 15th July 2011, Accepted 5th September 2011
DOI: 10.1039/c1ja10204d

The speed and effectiveness of a conservation treatment used for stained glass windows have been investigated. Dark-coloured Mn-rich stains can be found in the alteration layer of ancient glass artefacts and cause the surface to turn brown/black: this phenomenon is known as Mn-browning or Mn-staining. While in glass manganese is present in the +II or +III oxidation states, in the Mn-rich bodies, manganese is in a higher oxidation state (+IV). In restoration practice, mildly reducing solutions are employed to eliminate the dark colour and restore the clear appearance of the glass. In this paper the effectiveness and side effects of the use of hydroxylamine hydrochloride for this purpose are assessed. Archaeological fragments of stained glass windows, dated to the 14th century and originating from Sidney Sussex College, Cambridge (UK), were examined by means of synchrotron radiation (SR) based microscopic X-ray Absorption Near-Edge Spectroscopy (μ-XANES) and microscopic X-Ray Fluorescence (μ-XRF) and with high resolution computed absorption tomography (μ-CT) before, during and after the treatment. The monitoring of the glass fragments during the treatment allows us to better understand the manner in which the process unfolds and its kinetics. The results obtained reveal that the hydroxylamine hydrochloride treatment is effective, but also that it has a number of unwanted side effects. These findings are useful for optimizing the time and other modalities of the Mn-reducing treatment as well as minimizing its unwanted results.

Introduction

Glass alteration is a complex process governed by several factors and involving various transformations; an overview of this degradation process was recently described in detail by us elsewhere.[1] The speed and nature of the corrosion process depend both on the characteristics of the glass (*e.g.*, its composition, previous heat treatment, and surface roughness) and on external conditions such as microclimate, temperature, pH and composition of the aqueous solution the glass was in contact with and the exposed surface area of the glass. Also, the corrosion process can be influenced by micro-organisms, air pollution, exposure to sunlight, traffic vibrations, and earlier conservation treatments.[2]

The formation of brown-black Mn-rich corrosion bodies is one of the most disfiguring degradation phenomena that affect stained glass windows: a window pane that suffers from this phenomenon appears dark brown/black and completely lacks the transparency of the original glass. Mn-staining can appear both on archaeological glass and on *in situ* stained glass windows. Especially for stained glass windows reliable and harmless (for the glass and for the restorer) cleaning methods are highly needed.

Two factors are crucial for this alteration process: the presence of water (vapor or liquid) and a source of manganese in the direct vicinity of the glass fragment or inside the healthy glass itself. While it is easily understood that the Mn can originate *e.g.* from the ground water that surrounds a piece of window glass buried in soil, the effect of "internal" Mn usually cannot be neglected. Historical glass often contains a small amount of manganese, usually between 0.4 and 0.8% w/w (when expressed as MnO).[3] The most important fraction of manganese in healthy glass is in the Mn(II) state (colorless), while a minor fraction may be present as Mn(III) (purple). Higher oxidation states of Mn are generally not present in fresh glass, since they are unstable during glass production (*e.g.* above 900 °C). Mn can be introduced into glass in two ways: (1) as a raw material impurity (*e.g.*, because it was present in wood ash)[4,5] and (2) because of a deliberate addition

[a]*Department of Chemistry, University of Antwerp, Universiteitsplein 1, B-2610 Antwerp, Belgium. E-mail: simone.cagno@ua.ac.be; Fax: +32 32652376; Tel: +32 32652363*
[b]*Department of Industrial Chemistry and Materials, University of Bologna, Viale del Risorgimento 4, I-40136 Bologna, Italy*
[c]*Conservation Studies, Royal Academy of Fine Arts, Artesis University College of Antwerp, Blindestraat 9, B-2000 Antwerp, Belgium*
[d]*Karlsruhe Institute of Technology, P.O. Box 3640, D-76021 Karlsruhe, Germany*
[e]*ESRF, Rue Jules Horowitz, F-38043 Grenoble, France*
† This article is part of a themed issue highlighting the latest research in the area of synchrotron radiation in art and archaeometry.

(*e.g.*, as pyrolusite, MnO_2), usually for the purpose of acting as an oxidizing agent of Fe in order to eliminate the blue-green color caused by Fe(II) ('glass-makers soap').[6]

The presence of Mn in the superficial layers of historical glass has been investigated and reported in different research papers.[1,2,7–9] It is generally observed that in the dark areas within altered glass, manganese is present in the +IV oxidation state.[10,11] Silvestri *et al.*[9] reported the occurrence of zones rich in Mn, Ca, P and Fe in corrosion layers as typical for underground alteration. Moreover, it is known that in nature, Mn-oxides and manganates can be formed by either a chemical or a microbial oxidation of Mn(II) in the presence of water.[12] In restoration practice the Mn browning is treated by employing a solution of a (mild) reducing agent (such as citric acid or hydroxylamine hydrochloride).[13–16] In this way the manganese is reduced back from the higher oxidation states to the colorless Mn(II); the Mn(II) either remains in the superficial layers of the glass or dissolves into the reducing solution. However, experience has shown that it is difficult to eradicate the Mn-browning in a durable manner; the brown color can reappear relatively quickly, *i.e.* only a few years after the conservation treatment.

In our previous paper[1] we used a combination of Scanning Electron Microscopy coupled with Energy-Dispersive X-ray analysis (SEM-EDX), X-ray Computed Tomography (CT) and X-ray Absorption Near-Edge Spectroscopy (XANES) to investigate the morphology of the Mn-bodies and the oxidation state of the manganese *after* the corrosion process had taken place. On the basis of these observations, hypotheses could be formulated on the origin and formation mechanism of the Mn-browning. The scope of the present paper, instead, is to study the Mn-bodies *while* they are subject to the reducing and dissolving influence of a typical treatment solution, applied in conditions similar to those used in conservation/restoration. We do this by using relatively fast synchrotron radiation (SR) based imaging techniques that allow us to characterize either the surface (2D) or a sub-volume (3D) of the (corroded) glass fragment at different stages of its treatment. We consider this therefore to be a semi-continuous study, while our previous paper reported findings from a static investigation performed only before the treatment process.

In particular, this paper focuses on the removal of Mn-bodies by means of hydroxylamine hydrochloride solutions: desired and undesired effects of this conservation treatment on (a) the composition of the surface and (b) the structure of the glass fragments are recorded as the treatment progresses. This allows us to assess the speed and completeness of the treatment as a function of a number of parameters. The resulting information is useful to optimize the glass conservation/restoration procedure. To our knowledge, up to now no such study on the *treatment* of Mn-browning in historical glass, based on SR monitoring techniques, has been described.

In what follows, first, the results of μ-XANES measurements and μ-XRF mapping of the surface of corroded glass fragments at different stages during the reducing treatment are described. This allows us to qualitatively understand the nature of the physico-chemical transformations that occur and obtain an estimate of the speed with which they progress. In second instance, the results of the time-dependent 3D monitoring of the gradual dissolution of the MnO_2 bodies by means of high resolution μ-CT are discussed.

Background

(a) Glass weathering and Mn-browning. The weathering of silicate glasses is caused by a series of chemical reactions that take place in the presence of water.[17] The first step (1) is the penetration, *via* molecular diffusion and/or reversible hydrolysis/condensation reactions, of molecular water into the glass, inducing structural transformations in the silica network.[18,19] For glass buried in a wet environment, ppm amounts of molecular water diffuse into the glass surface causing silicon–oxygen bonds to break and form:[20]

$$\begin{aligned} &\equiv Si - O - Si\equiv + H_2O_{(aq)} \rightarrow 2\equiv Si - OH \\ &2\equiv Si - OH \rightarrow \equiv Si - O - Si\equiv + H_2O_{(glass)} \end{aligned} \quad (1)$$

In a second step (2), occurring at low pH values, ion exchange takes place: the most mobile cations (*i.e.*, monovalent ions such as Na^+ and K^+) are leached from the glass and become substituted by protons (see Fig. 1a).[21–23] Since the mobility of cations depends on their charge, size and on the glass composition itself, some glass types (such as silica-rich glasses) are more resistant to leaching than others. During the exchange process, the density of the leached layer becomes lower than that of the original glass. The ions removed from the glass structure can also form weathering products (typically sulfates and chlorides of Ca, Mg, *etc.*) on the glass surface.[11,24–26]

$$\equiv Si{-}O^-M^+_{(glass)} + H^+_{(aq)} \rightarrow \equiv Si{-}O^-H^+_{(glass)} + M^+_{(aq)} \quad (2)$$

When the water that is in contact with the glass surface is not regularly replenished (as is the case during alternate wet/dry conditions), the local pH will increase due to the ongoing ion-exchange. When pH values exceed 9, the third step of glass weathering can occur (3), involving the attack of the silicate network by hydroxyl ions.[1]

$$\begin{aligned} &\equiv Si - O - Si\equiv + OH^-_{(aq)} \rightarrow \equiv Si - OH + \equiv Si - O^- \\ &\equiv Si - O^- + H_2O_{(aq)} \rightarrow \equiv Si - OH + OH^-_{(aq)} \end{aligned} \quad (3)$$

The three aforementioned steps cause a leached layer to be formed, consisting of a cation-depleted silica network that is structurally weakened and that has a lower density than the original glass. If no change in environmental conditions occurs, this leached layer (or gel layer) gradually increases in thickness. As its thickness becomes larger, the stress across the interface between altered and healthy glass increases, causing a thin layer of cation-depleted glass to crack off. This physical process in turn exposes a new surface of unaltered glass to the weathering agents. By a succession of such events, stacks of μm thin lamellae of

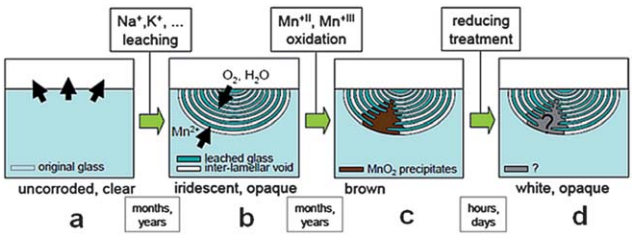

Fig. 1 Scheme representing the multi-step corrosion of historical glass, leading to Mn-browning, and its conservation treatment.

leached-out glass, interspersed with voids, can be formed (*e.g.*, in the form of hemispherical corrosion bodies, see Fig. 1b). Due to optical interference phenomena, the multilayered material can obtain an iridescent aspect when the inter-lamellar voids dry out.

As stated elsewhere in more detail,[1] as part of the leaching process, a flux of Mn-ions emerges from the healthy glass that may remain dissolved in the solution that is present in the inter-lamellar voids. In the presence of water and oxygen, the Mn-ions, originally predominantly present in the +II oxidation state, can be oxidized to higher oxidation states, giving rise to, for instance, insoluble MnO_2 that can subsequently precipitate following equilibrium (4). The Mn-precipitates, located in the cracks and voids within the multi-layered alteration layer (Fig. 1c), give the glass surface an unwanted dark appearance, particularly noticeable in figurative stained-glass windows.

$$Mn^{2+} + {}^1/_2\, O_2 + H_2O \rightleftharpoons MnO_2\downarrow + 2H^+ \qquad (4)$$

(b) Conservation treatments for Mn-browning. Up to now, only a limited number of papers on the treatment of historical glass affected by manganese staining have been published.[13–16] The use of solutions of different reducing and chelating agents at various concentrations is reported: hydroxylamine hydrochloride, hydroquinone, citric acid, potassium iodide and EDTA. However, the most commonly used products are hydrazine[16,27] and a commercial product containing hydrazine and hydroxylamine hydrochloride.[28]

When these products are applied to the leached layer, in a relatively short time (*e.g.*, after 1–2 days of exposure) the brown stains disappear and the leached layers obtain a semi-transparent, whitish aspect (Fig. 1d). From optical microscope observations (Fig. 2) of a Mn-browned glass fragment at different stages of treatment with hydroxylamine hydrochloride 5% w/w (0–15–30 minutes) it is clear that a change in the shape and distribution of the Mn-bodies occurs: for instance the grape-shaped structure visible in the untreated sample disappears at the following stages, while the hemispherical bodies near the surface remain in place. The exact nature of the transformations that occur during the reducing treatment is not known; however we can assume that reduction of Mn from the +IV to a lower valence state takes place. Apart from this reduction *per se*, it is unclear whether all or part of the reduced Mn remains in place inside the same or other areas of the leached layer, or is totally extracted from the glass into the reducing solution. In case the Mn remains in place after the reducing treatment, the possibility exists that the Mn-staining will gradually reappear due to spontaneous re-oxidation. On the other hand, if all or most of the Mn is dissolved and removed from the glass, the Mn-depleted leached layer that results is likely to be very prone to invasion by dissolved ionic species from the environment and for this reason may again lose its restored aspect over time. The latter may also be caused by diffusion of Mn from the still healthy parts of the glass that are in contact with the leached layer (see Fig. 1b). The present paper therefore also tries to increase the insight into what exactly is the fate of the Mn contained in the brown corrosion bodies immediately after the reduction, with the final aim of providing guidelines for a (more) durable conservation approach for corroded glass.

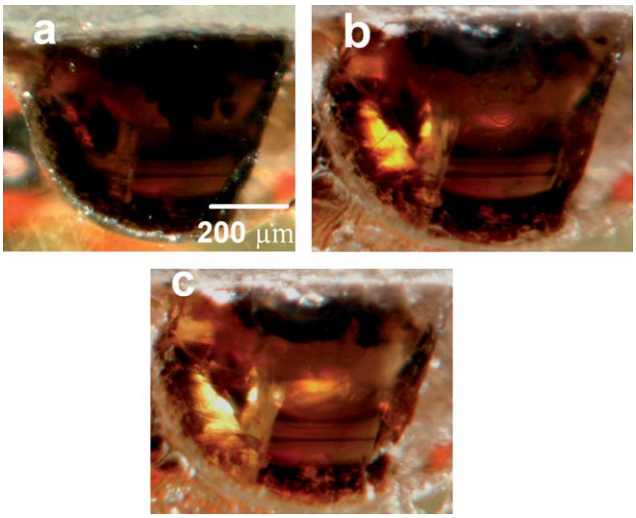

Fig. 2 Sidney Sussex College sample, cross-section of a superficial area (a) untreated, (b) treated with hydroxylamine hydrochloride 5% for 15 minutes, and (c) treated with hydroxylamine hydrochloride 5% for 30 minutes.

Materials and methods

(a) Corroded glass material

The experiments described below were conducted on original material without art-historical value. Historical glasses—especially those originating from antiquity and the Middle Ages—are mostly retrieved from archaeological excavations. Among these finds, there are fragments that are not easy to reassemble or that are not particularly significant or overrepresented in an archaeological assemblage. These pieces are stored in depots and are available for scientific investigations upon request. The samples studied in this research came from an archaeological site in Sidney Sussex College, Cambridge (UK), a former Franciscan friary.[29] The glass fragments were part of several stained glass windows that date to the 14th century; they suffered corrosion in a wet environment (groundwater) for about four centuries. Among the available historical glass fragments, the Sidney Sussex College finds were selected because of their extensive Mn-browning and because of their composition, typical of a glass of low intrinsic durability, characterized by low silica (SiO_2) and high potash (K_2O) content (Table 1). The glass composition was determined *via* SEM-EDX analyses; more information on the technique and quantification procedure is provided elsewhere.[30]

(b) Methods of analysis

Three synchrotron radiation (SR) based techniques were used: (a) microscopic X-ray Absorption Near-Edge Spectroscopy (μ-XANES), in order to determine the oxidation state of manganese before and after the treatment, (b) microscopic X-Ray Fluorescence (μ-XRF) at different primary energies in the Mn-K edge region, in order to qualitatively map the distribution of the different oxidation states of manganese at different treatment stages, and (c) computed X-ray absorption micro-tomography (μ-CT), in order to study the morphology of the alteration layer and the different phases that can be distinguished

Table 1 Sidney Sussex College samples, bulk glass composition (% w/w), average and standard deviation of four measurements

Sample	Na_2O	MgO	Al_2O_3	SiO_2	P_2O_5	K_2O	CaO	MnO	Fe_2O_3
C2	2.7 ± 0.2	5.2 ± 0.3	1.9 ± 0.1	55.6 ± 0.4	2.9 ± 0.1	12.4 ± 0.1	16.9 ± 0.2	0.8 ± 0.1	0.8 ± 0.1
C9	3.0 ± 0.3	8.7 ± 0.1	1.6 ± 0.1	52.5 ± 0.2	3.3 ± 0.1	11.5 ± 0.1	16.6 ± 0.2	1.6 ± 0.1	0.6 ± 0.1
C10	0.4 ± 0.2	4.9 ± 0.3	0.8 ± 0.2	48 ± 1	1.4 ± 0.1	17.9 ± 0.7	23.6 ± 0.3	1.6 ± 0.1	0.6 ± 0.2
C12	0.2 ± 0.2	4.5 ± 0.3	1.3 ± 0.4	47.0 ± 0.2	2.5 ± 0.1	15.8 ± 0.3	27.2 ± 0.4	0.5 ± 0.1	0.4 ± 0.1

within. The experiments were done at the European Synchrotron Radiation Facility (ESRF, Grenoble, France), at beamline ID21 (μ-XANES and μ-XRF) and ID19 (μ-CT).

Beamline ID21 is devoted to X-ray and infrared microscopy; it houses two microscopes: a Scanning X-ray Microscope (SXM) and an infrared microscope (SR-FTIR microscope). The SXM, used for this study, operates in the primary energy range from 2.1 to 9 keV. A Si(111) fixed-exit double-crystal monochromator was used to produce a highly monochromatic primary beam. μ-XANES and μ-XRF experiments were performed in vacuum (10^{-6} mbar), in order (i) to minimize air absorption (which is significant for light elements and for low-energy X-ray fluorescence lines) and (ii) to avoid contributions to the spectral background due to scattering in air. The beam-size was reduced from 0.2 mm diameter with a pinhole to *circa* 0.3 × 0.8 μm^2 with a Kirkpatrick–Baez mirror system. For the acquisition of μ-XANES spectra, the beam was slightly defocused to ~10 × 10 μm^2 in order to eliminate the photo reduction that was observed when exposing the samples to the sub-micrometric beam. A Silicon Drift Diode (SDD) detector (Röntec) was used to collect X-ray signals. μ-XANES spectra were acquired by scanning the primary energy range (6.52–6.63 keV) around the Mn K-edge with a step size of 0.55 eV. The energy calibration was performed using a Mn foil. For all XANES spectra, the procedure of normalization was performed by means of ATHENA, a software package widely used for (E)XAFS data analysis. In particular, edge-step normalization of the data was performed by means of linear pre-edge subtraction and by regression of a quadratic polynomial beyond the edge.[31] Prior to the sample analysis, reference XANES spectra were acquired in transmission and fluorescence mode on pure Mn-compound powders and Mn-containing glasses. Selected glass samples were then measured: the analyses were done on the same area, before and after a 30 minute treatment with hydroxylamine hydrochloride 2% w/w in deionized water.

The μ-XRF signals were collected in the vertical plane and perpendicular to the primary beam by means of the same SDD detector used for μ-XANES. This device is characterized by a resolution of 130 eV at 6 keV and a limit of detection (from P to Fe) of approximately 10 ppm. Both the setup and the procedure for evaluation of XRF spectra are discussed in more detail elsewhere.[32] During the μ-XRF mapping experiments, the fluorescence signals were generated by employing a monochromatic primary beam at fixed energies (6.550 keV for Mn^{2+}, 6.558 keV for Mn^{4+}, and 6.587 keV for the higher oxidation states—see Fig. 2) chosen after observing the Mn-K-edge XANES spectra, in order to differentially excite the oxidation states of Mn that were the object of investigation. During map collection the focussed beam (0.3 μm × 0.8 μm) was used, considering the short collection time per point (200 ms). The step size was 1 μm. The PyMCA software was used to fit the fluorescence spectra corresponding to each pixel of the two-dimensional (2D) maps.[33]

The μ-CT experiments were performed at beamline ID19. This beamline was specifically designed for X-ray imaging with a (sub) micron resolution. The monochromaticity of the beam is obtained with a multilayer monochromator (with a relative energy bandwidth $\Delta E/E$ of *ca.* 10^{-2}) and contributes considerably to improving the contrast between the various phases present in the sample.[34] The detector system consists of an X-ray to light converter (scintillator) with an optical system (mirror and lenses) to project the magnified image onto the sensor chip of a Charge-Coupled Device (CCD) camera. For the CT experiments, a FRELON (Fast REadout LOw Noise) CCD camera with 2048 by 2048 pixels was used, that is designed and produced at the ESRF. This 14-bit depth resolution CCD camera allows fast acquisition of radiographs with good quality, and high magnification. The glass samples were scanned with a beam energy of 19 keV. Using this optics configuration, for each tomographic scan, 1500 projections were acquired over a rotational range of 180°, with an effective pixel size of 700 nm. These conditions were selected because they offer a good balance between image quality and scanning time (approximately 10 min per scan). Finally, the volumes were reconstructed *via* a filtered backprojection algorithm,[35] based on Radon's theorem.[36] Each historical glass sample was scanned before, during and after treatment. In order to maximize the available analysis time and minimize the time spent on sample handling, the treatment was monitored in a semi-continuous way: the samples were first placed into a 2% w/w hydroxylamine hydrochloride solution; after a specific exposure time (30 minutes) they were removed and a CT scan was performed.

After the μ-CT measurement (taking *ca.* 10 min), the samples were returned into the solution for a further 30 min treatment and subsequently reanalyzed, and so on. The treatment solution was not refreshed in order to approximate the conditions of a continuous (*i.e.*, uninterrupted) treatment. The total time covered by this semi-continuous treatment was 270 minutes, *i.e.*, in addition to the first CT-scan documenting the initial 3D morphology of the glass fragments, 9 cycles involving treatment and CT-imaging were performed.

Results

(a) XANES measurements

As explained before, the first part of the experiment involved the visualization of the change in the oxidation state of Mn in the Mn-deposition areas and in the neighboring areas of the samples by means of XANES, before and after the treatment with hydroxylamine hydrochloride. Before performing the actual

measurements, the effect of the incident synchrotron beam on the samples was evaluated. Beam-induced reduction/oxidation of different chemical species is often reported in the literature.[37,38] During our measurements, photo-reduction of the more oxidized forms of Mn towards Mn(II) was effectively observed in the historical glass at the ESRF-ID21 end station, when a KB-focused beam (*circa* 0.3 μm × 0.8 μm) was used for sample excitation. A relatively rapid shift of the XANES edge position towards lower energies was registered when performing subsequent XANES spectrum collections on the same spot in the Mn-precipitation area; the effect was already visible after a total irradiation time of 60 s on the same sample position. To overcome this problem, a defocused beam (10 μm diameter) rather than a submicron beam was employed for the collection of the XANES spectra. With this beam, no observable photo-reduction took place during the times required to collect the XANES spectra shown in Fig. 3.

In Fig. 3 the Mn-K edge XANES spectra obtained from different positions in a Mn-precipitation area (spectrum 4), the leached layer (spectrum 5) and the healthy glass (spectrum 6) are shown, before (below) and after treatment (above) with a 2% hydroxylamine hydrochloride solution for 30 min. This figure also shows the spectra of Mn-reference compounds (spectra 1–3). The difference in the spectra of the Mn-precipitation layer before and after treatment clearly demonstrates that the (majority of the) Mn is indeed reduced by the hydroxylamine hydrochloride. Both the shifts of the edge towards lower energy and the change in shape point this out: before the treatment the XANES spectrum of the Mn-precipitation area (spectrum 4) resembles that of MnO_2 (a broad white line with maximum near 6560 eV—see the line on the right in Fig. 3) while afterwards, a sharper white line with a maximum near 6550 eV (line on the left in Fig. 3), similar to that of $MnSO_4$, is obtained.

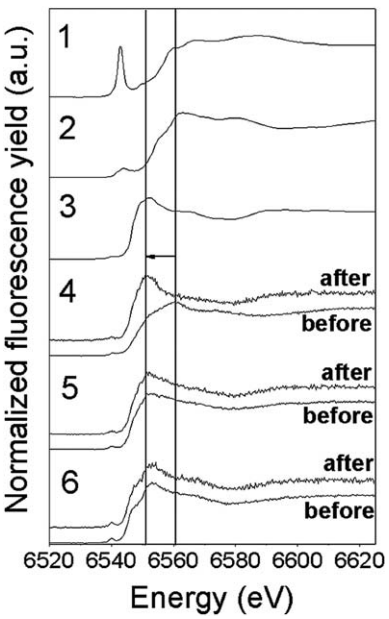

Fig. 3 Mn–K-edge XANES spectra of reference compounds (1: $KMnO_4$; 2: MnO_2; 3: $MnSO_4$) and of different areas of a corroded glass sample before (lower spectra) and after treatment (upper spectra): (4) Mn-precipitation area; (5) leached layer; and (6) healthy glass. Treatment: 30 min exposure to a hydroxylamine hydrochloride 2% w/w solution.

It is the first time that the effect of this type of treatment is experimentally shown by XANES measurements. The remaining spectra in Fig. 2 (spectra 5 and 6) show that the treatment does not significantly affect the oxidation state of Mn in the other areas (alteration layer, healthy glass) of the examined samples. In these areas the Mn-atoms still form a part of the Si-network.

A future step of the study will be the quantitative determination of the oxidation state of Mn in the different parts of the samples; different approaches for this are proposed, from linear combinatorial fitting to pre-edge analysis.[39,40] However, the quantitative investigation of the Mn-valence and the equilibria between possible different Mn(II), Mn(III), Mn(IV), Mn(VI) and Mn(VII) species inside the Mn-bodies is beyond the scope of this paper and is planned to be examined in greater detail and on a larger number of samples elsewhere. In the context of the present study, relative to the evaluation of the reducing treatment, we limit ourselves to conclude that hydroxylamine hydrochloride effectively reduces the valence of the Mn originally present in the Mn-bodies from higher oxidation states to the +II level.

(b) μ-XRF based elemental and Mn-species specific mapping

After the qualitative determination of the oxidation state(s) of the different types of Mn present *via* μ-XANES, their distribution at the surface of the glass was visualized by selecting different primary beam energies (E_0) in order to favor the excitation (and resulting emission of element specific radiation) of Mn in a particular oxidation state. In order to determine the minimum number of different E_0 values required to completely characterize the samples during the treatment, a series of Mn-K_α maps were recorded at different energies. This involves the collection of XRF spectra at each of the pixels comprised in the mapped areas, followed by extraction of the net Mn-K_α intensities at each position. In Fig. 4a–c, a subset of these maps is shown, *i.e.*, the intensity distributions:

$$I^{\mathrm{Mn}}_{E_0=6.550\ \mathrm{keV}}(x,y);\quad I^{\mathrm{Mn}}_{E_0=6.558\ \mathrm{keV}}(x,y);\quad I^{\mathrm{Mn}}_{E_0=6.587\ \mathrm{keV}}(x,y)$$

As is evident from Fig. 3, when the primary energy is 6.550 keV, Mn in the +II form is optimally excited; however, also the +IV oxidation state of Mn is somewhat excited at this energy. At higher energies (6.558 keV), besides Mn(II), Mn in the +IV form is more efficiently excited while at $E_0 = 6.587$ keV, *i.e.*, well above the Mn-K edge, all species of Mn are excited with equal probability. The maps of Fig. 4a–c show a significantly different distribution at $E_0 = 6.550$ keV than at $E_0 = 6.558$ keV; on the other hand, no significant new contribution is observed when higher excitation energies than 6.558 keV (the maximum of excitation efficiency for MnO_2) are employed. It can be concluded that, prior to treatment, mainly two Mn species are present in the glass, henceforth denoted as Mn(II) and Mn(IV), and that these two can be visualized in a satisfactory manner by recording Mn-K_α maps at 6.550 and 6.558 keV only. These maps both are weighted sums of the distributions of the Mn(II) and Mn(IV) species.

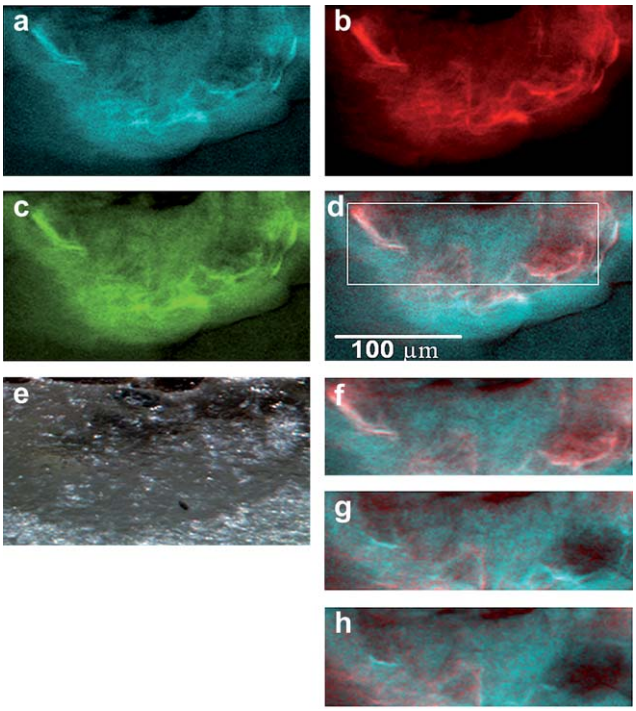

Fig. 4 As-recorded Mn-K$_\alpha$ intensity maps at (a): $E_0 = 6.550$ keV, (b): $E_0 = 6.558$ keV and (c): $E_0 = 6.587$ keV; (d): RC composite [Red: Mn(IV); Cyan: Mn(II)] map showing the Mn(II) and Mn(IV) species distribution in the untreated sample; (e): optical microscope image of the analyzed area (taken after treatment); and (f–h): RC composite [Red: Mn(IV); Cyan: Mn(II)] maps showing the evolution *vs.* time (f: 0 min, g: 30 min, h: 60 min treatment) of the Mn(II) and Mn (IV) species distribution; examined area (66×181 μm^2) shown in the dashed rectangle in (d).

To estimate the relative contribution of each Mn species at the two different energies, chemical species-specific sensitivity factors (S) were introduced, in order to describe the different efficiency with which both Mn-species are ionized at the two different E_0 values. These S factors relate the observed Mn-K$_\alpha$ X-ray intensity (I) in the sample at a given primary energy E_0 to the irradiated masses of two Mn-species $m_{\mathrm{Mn(II)}}$ and $m_{\mathrm{Mn(IV)}}$ present at that location, following this relation (5):

$$I_{E_0}^{\mathrm{Mn(unk)}} = S_{E_0}^{\mathrm{Mn(II)std}} m_{\mathrm{Mn(II)}} + S_{E_0}^{\mathrm{Mn(IV)std}} m_{\mathrm{Mn(IV)}} \quad (5)$$

The sensitivity factors can be defined as the XANES intensity readings of the respective Mn-reference compounds at E_0. Thus, from a Mn-K$_\alpha$ X-ray intensity map, at each given position (x,y) the $\mathrm{m_{Mn(II)}}$ (x,y) and $\mathrm{m_{Mn(IV)}}$ (x,y) Mn-oxidation state specific maps (these maps are shown in Fig. 4d, f, g and h) can be extracted from the following matrix equation.

$$\begin{pmatrix} I_{E_0=6.550\ \mathrm{keV}}^{\mathrm{Mn(unk)}}(x,y) \\ I_{E_0=6.558\ \mathrm{keV}}^{\mathrm{Mn(unk)}}(x,y) \end{pmatrix} = \begin{pmatrix} S_{E_0=6.550\ \mathrm{keV}}^{\mathrm{MnSO_4}} & S_{E_0=6.550\ \mathrm{keV}}^{\mathrm{MnO_2}} \\ S_{E_0=6.558\ \mathrm{keV}}^{\mathrm{MnSO_4}} & S_{E_0=6.558\ \mathrm{keV}}^{\mathrm{MnO_2}} \end{pmatrix} \times \begin{pmatrix} m_{\mathrm{Mn(II)}}(x,y) \\ m_{\mathrm{Mn(IV)}}(x,y) \end{pmatrix} \quad (6)$$

In this model we assumed that the sensitivity of Mn(II) and Mn(IV) at both energies can be derived with good approximation from the $MnSO_4$ and MnO_2 reference XANES spectra. The sensitivity values are therefore defined as the intensity readings of the XANES spectra of the $MnSO_4$ and MnO_2 standards at the two E_0 values, normalized to the observed intensity far above the edge.

It should be noted that this type of calculation is approximate in nature only and leads to the semi-quantitative maps shown in Fig. 4d,f–h; however, we consider them to be sufficient for the present purpose. In order to be able to monitor the effect of the reducing treatment on the Mn(II) and Mn(IV) distributions with sufficient time resolution, a smaller area than the one shown in Fig. 4a–c was repeatedly scanned, comprising fresh glass, altered glass and a Mn-deposition area. In Fig. 4e, a photograph of the surface of the sample after treatment is shown: the interface between the leached layer and the bulk glass is clearly visible. Maps were collected at the following stages of a 2% hydroxylamine hydrochloride treatment: no treatment, one treatment of 30 minutes and two treatments of 30 minutes. In Fig. 4d, a composite map of the $m_{\mathrm{Mn(II)}}$ and $m_{\mathrm{Mn(IV)}}$ distributions obtained before the treatment is shown (resp. in cyan and red). The distribution of oxidized Mn in the Mn-precipitation area is clearly visible. In a similar manner, $m_{\mathrm{Mn(II)}}$ and $m_{\mathrm{Mn(IV)}}$ distributions after 0, 30 and 60 min of exposure are shown in Fig. 4f–h (66×181 μm^2).

By comparing the $m_{\mathrm{Mn(IV)}}$ distributions in Fig. 4f–h, it follows that a substantial amount of Mn(IV) (and possibly in higher oxidation states) that is originally present in the Mn-containing corrosion bodies is already reduced after 30 min, agreeing with the μ-XANES results. However, after 60 minutes there is still a residual presence of oxidized Mn in the deposition area. We can therefore conclude that it is relevant to monitor the reducing treatment during a longer period of exposure.

Moreover, it is also possible to qualitatively monitor the removal of Mn at the different steps of the treatment, by observing the Mn maps of the same region collected at $E_0 = 6.558$ keV, where both Mn +II and +IV are excited. By observing Fig. 5 it is clear that the brighter structures in the left and right part of Fig. 5a are already removed in the first 30 minutes of treatment (Fig. 5b), while only small changes can be observed in Fig. 5c (60 minutes). When comparing these images with Fig. 4f–h, it is clear that the removed Mn-bodies are those containing the highest relative amount of Mn(IV) (shown in red in Fig. 4f–h). It is clear that Mn is still present in the alteration layer. The remaining Mn can be of three types: (a) Mn(IV) in the Mn-deposition areas; (b) former Mn(IV) reduced to Mn(II) by the treatment but not solvated; and (c) Mn(II) contained in the glassy structure of the leached layer.

(c) Computed tomography monitoring of the conservation process

CT allows the visualization of the inner structure of objects, by virtually reconstructing the sample volume, represented in tones of gray that are directly correlated with the X-ray attenuation coefficient of the different materials present in the object.

All the examined glass samples yielded very similar results in terms of average X-ray attenuation coefficient of the healthy glass and of the leached layers. As an example, in Fig. 6, we present (within a 1.4 mm × 1.4 mm × 0.7 mm parallelepiped) a combination of one transverse and three longitudinal planes inside the same sample, after treatment during resp. 0 treatments (*i.e.*, condition before any treatment), 6 treatments, each of

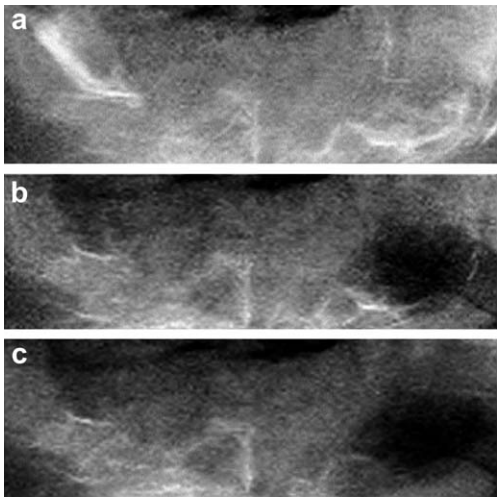

Fig. 5 Series of three maps acquired at $E_0 = 6.558$ keV, showing the Mn distribution in the same area shown in Fig. 4f–h, (a) in the untreated state, (b) after treatment of 30 minutes with hydroxylamine hydrochloride 2%, and (c) after treatment of 60 minutes with hydroxylamine hydrochloride 2%. Being both Mn(II) and Mn(IV) excited at the selected energy, these maps can be used to qualitatively observe the total amount of Mn removed by the treatment.

30 min and 9 treatments, each of 30 min. These images clearly reveal the progression of the treatment: the high density areas (Mn-rich deposits), represented in the whiter tones, distinctly shrink as a function of increasing treatment time. To our knowledge, it is the first time that the progressive removal of Mn-bodies in historical glass has been visualized by means of high resolution SR-CT.

It is relevant to mention that, in those locations where the manganese has been reduced, sub-volumes with a similar absorption coefficient than that of the surrounding leached-out glass are observed. This shows that Mn is not simply reduced, but also dissolves into the reducing solution, probably because the resulting Mn(II)-ions are immediately solvated and readily diffuse out of the leached layer. On the basis of the tomograms, 3D models of selected areas of the samples were created by selecting only the voxels having a density/attenuation coefficient within a specific range of values. Some results are shown in Fig. 7. By inspecting the 3D model, one can appreciate more finely the hemispherical shape of the Mn-bodies and evaluate their interconnections. In Fig. 7 the evolution of a sub-volume of 494 μm × 231 μm × 763 μm, in which several Mn-precipitates were present, is shown. The precipitates are associated with a linear absorption coefficient that is significantly higher than that of the surrounding glass. The gradual shrinking of the volume of the precipitate body with time is evident. The removal of Mn towards the outside evidently takes place through a crack (see arrows in Fig. 7) that connects the subsurface part of the precipitate body with the glass surface.

An important undesired effect of the treatment could also be visualized by means of SR-CT. In Fig. 8, three tomograms of the same area of a sample at different treatment stages are shown: it concerns an area where originally only healthy glass (albeit fragmented) is present. The tomograms clearly show that on all surfaces of the glass that was exposed to the solution, a leached layer (of lower absorption coefficient) develops. This is especially the case not only on the outer surface of the examined glass fragment but also (albeit to a lesser extent) on the inner surfaces of the cracks.

After 270 min of exposure to the solution, the thickness of the outer alteration layer reaches *ca.* 30 μm. The water and the acidic conditions (pH 3–4), favouring the leaching of cations, due to the application of the 2% w/w hydroxylamine hydrochloride solution, are the most important agents promoting the alteration; also the corroded and fissured nature of the analyzed glass fragments accelerates the weathering.

The expansion of the leached layer can be visualized better by employing a 3D model of the external surface of a glass fragment at different treatment stages (Fig. 9). It is evident from the picture that a sizeable volume of the formerly healthy glass (light gray) suffers alteration when it comes (and is maintained) in contact with water. It can also be observed how the expansion of the leached layer (dark gray) evolves in two directions: from the surface into depth, and along the cracks. It appears that the expansion in depth is faster in the first period (the newly created leached layer is permeable to water), while at longer treatment times water penetrates (and thus alteration occurs) through preferential ways such as micro-cracks and fractures.

In order to estimate the speed of Mn-removal, the volume fraction taken up by the Mn-rich bodies and by the leached-out glass can be calculated in each CT dataset and plotted as a function of the treatment time (Fig. 10). The Mn-bodies volume appears to diminish with time following first order reaction kinetics (exponential decay), with a half-life of approximately 50 minutes. Such behaviour would be observed when the amount of Mn removed per unit of time would be proportional to the total amount of (precipitated) Mn present. Thus, more than half of the initial total volume of Mn-precipitate is removed within the first hour of treatment, while after this initial phase, the speed tends to diminish, leaving a non-dissolved fraction of *ca.* 0.8% of the imaged volume after 270 minutes. This corresponds to *ca.* 11% of the original volume taken up by the Mn-precipitates. The gradual expansion of the volume of the leached-out glass is also shown in Fig. 10. As a function of exposure time, the volume of the gel layer appears to increase in time at constant speed, increasing from *ca.* 12 to *ca.* 15% of the total imaged volume; thus, this corresponds to a relative increase of the volume of the gel layer with *ca.* 25%, which is quite significant.

Discussion and conclusions

After evaluating the qualitative and semi-quantitative results of the different methods of analysis employed in this study, a number of deductions can be made. Consistent with previous observations, from the μ-XANES results and the μ-XRF maps, it can be deduced that the manganese, located in the deposition areas below the glass surface, is present in a more oxidized form than in the glass or the surrounding leached layer. Upon application of the hydroxylamine hydrochloride solution, the first process to take place is the reduction of Mn from the more oxidized forms to water-soluble Mn(II) compounds. This is indeed the desired effect of the conservation treatment.

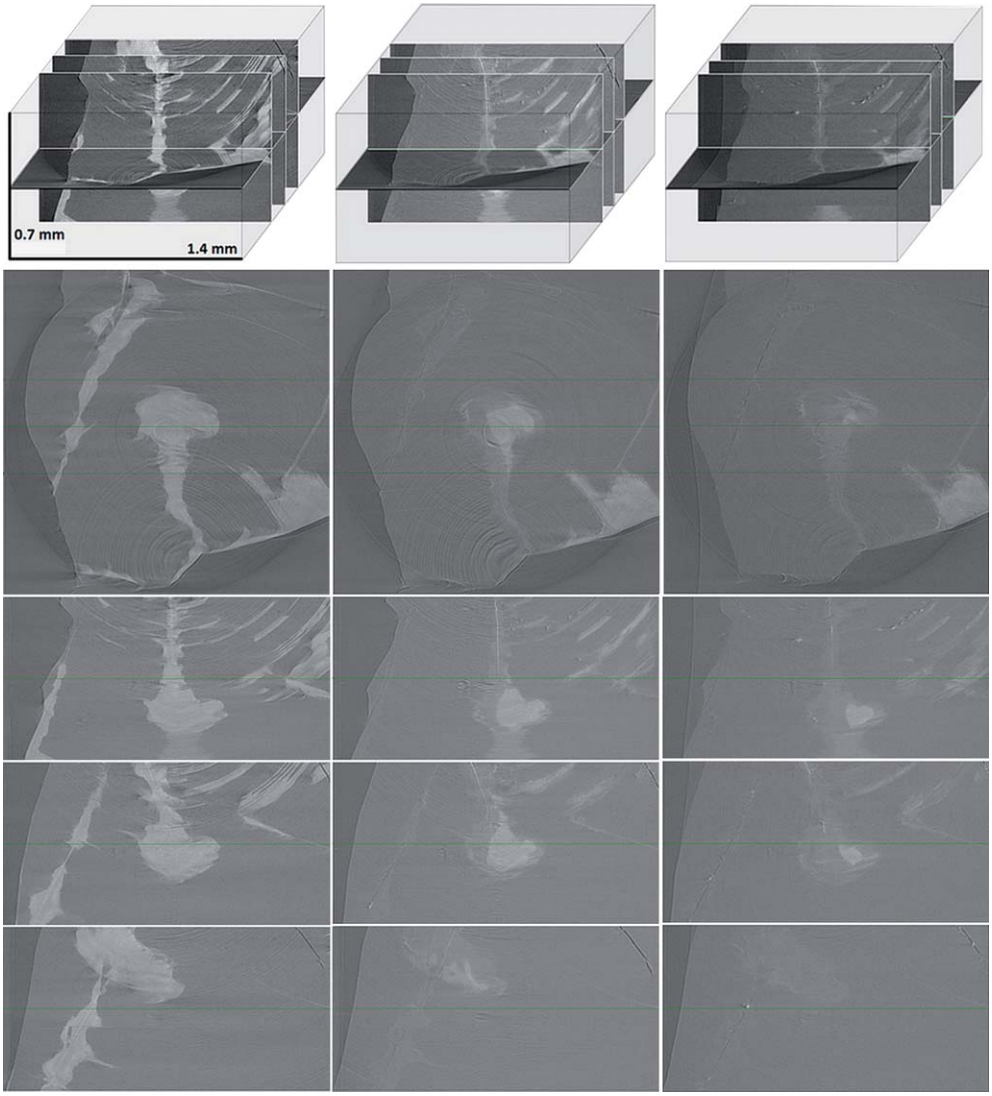

Fig. 6 Tomograms (from the top: scanned volume, one transverse plane, three longitudinal planes) showing the same sample at different treatment times: 0 min (left), 180 min (middle) and 270 min (right). Green lines indicate the relative position of the longitudinal planes in the transverse section and *vice versa*. Plane sizes: 1.4 mm × 1.4 mm (transverse) and 1.4 mm × 0.7 mm (longitudinal).

At this point, as the CT results show, the removal of Mn from the glass samples towards the solution starts at a high rate; this rate gradually decreases with the difference in Mn-concentration (and chemical potential) between the leached layer and the solution. The tomograms and 3D models demonstrate that SR-CT is a very powerful method to visualize and monitor the effect of the treatment. The absorption coefficient of the sub-volumes formerly occupied by the Mn-rich bodies resembles that of the surrounding leached layer, indicating that no voids are created in these locations.

It is important to mention that, after employing the longest treatment time (270 minutes), a fraction of Mn still remained in the alteration layer. This may be due to an incomplete penetration of the solution in the inner parts of the leached glass. However, one must take into account that the repeated interruption of the treatments, accompanied by a partial drying-out of the samples due to the irradiation during the CT-scans, may have influenced these results. From a conservator's point of view, the incomplete removal of Mn evidenced by this study might account for most of the short-lived restorations of Mn-browned glass.

Finally, an undesired aspect of the treatment becomes clearly visible: leaching damage is inflicted to the original glass by the reducing solution. Previously non-corroded surfaces develop gel layers and the dimensions of the cracks present in the historical glass are expanded by the exposure to the aqueous solution; this effect is proportional with time: after 270 minutes a 25% increase of the leached layer volume was registered. The fact that such damage takes place is not surprising, taking into account the nature of the treatment. However, considering that the use of these types of solutions is fairly common in restoration practice, some precautions should be taken. Expansion of the leached layer is extremely harmful, not only because it eliminates original historical material, but also because it might compromise in an irreversible manner the stability and the integrity of the entire glass object.

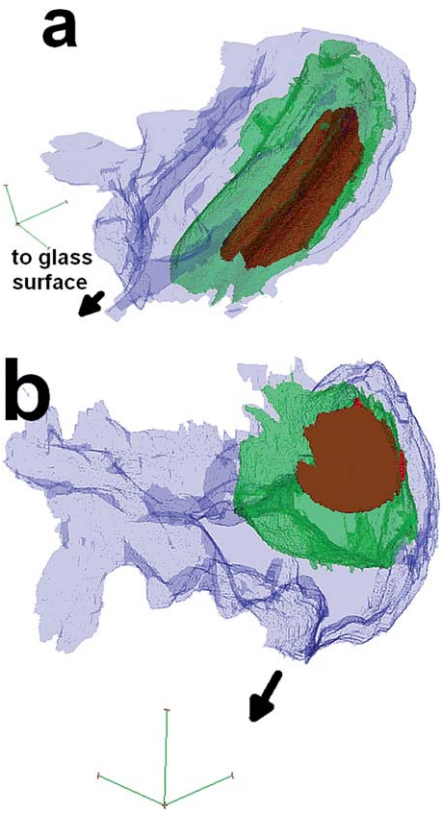

Fig. 7 Combined 3D-rendering of a selected Mn-body volume at treatment time of 0 min (blue), 180 min (green) and 270 minutes (red). (a) Longitudinal plane view; (b) transverse plane view (see from beneath). Size of volume shown: 494 μm × 231 μm × 763 μm.

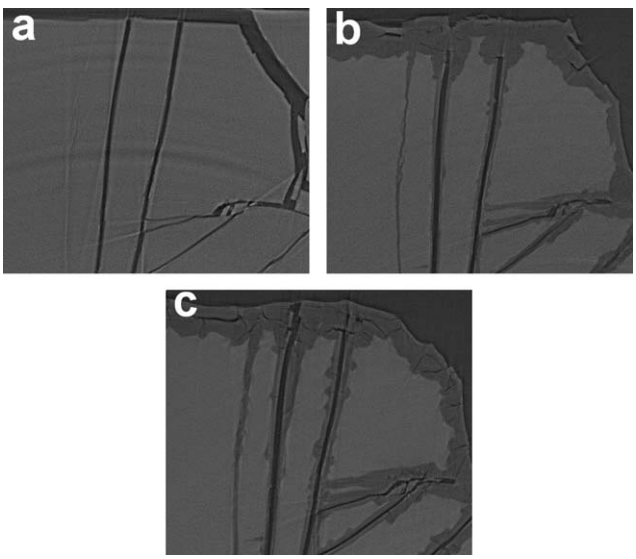

Fig. 8 Tomograms (400 μm × 340 μm) showing a detail of the expansion of alteration layer and cracks at different treatment times: (a) 0 min, (b) 180 min, (c) 270 min.

Summarizing, on the basis of these deductions, two important dynamics have to be considered when performing this conservation treatment:

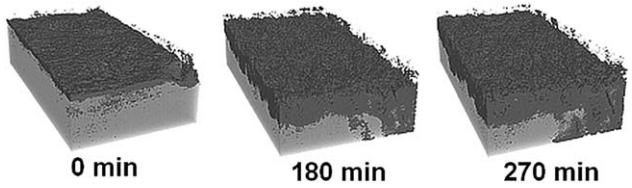

Fig. 9 3D models of the sample surface showing the growth of the leached layer thickness with increased treatment time (light grey: healthy glass, dark grey: altered glass). A subvolume of 100 μm × 50 μm × 180 μm is represented. The average thickness of the leached layer increases from 5 μm (0 min) to 15 μm (180 min) and 18 μm (270 min).

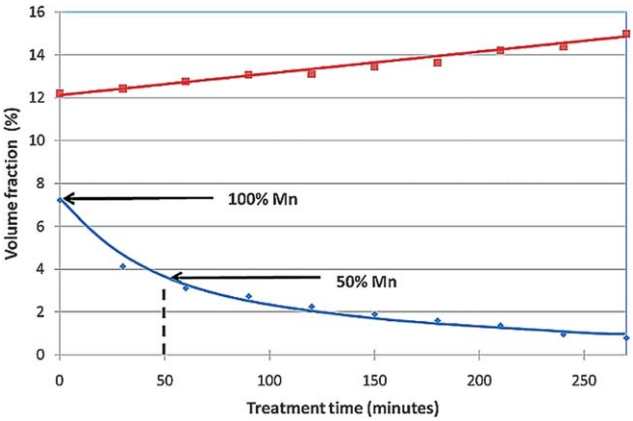

Fig. 10 Volume fraction of Mn-rich precipitation bodies (blue, ◇) and of the leached layer (red, ■) volume fraction *versus* treatment time.

a) Speed and efficiency of Mn-removal: the treatment time and/or hydroxylamine hydrochloride concentration may need to be increased in order to fully remove the Mn-bodies and prevent further alteration/re-oxidation of the Mn that remains behind.

b) Speed and efficiency of glass leaching/gel layer formation: measures need to be taken in order to prevent undesired alteration induced by the contact with the reducing solution. This might be realized, *e.g.*, by employing hydroxylamine hydrochloride solutions (more) saturated with alkali and/or alkaline-earth ions, so that they are less prone to extract these ionic species from the glass.

Optimal conditions that maximize Mn-removal while minimizing undesired cation leaching need to be identified. Since performing the treatment within a shorter time is not possible, because it will not allow the complete elimination of Mn, alternative approaches need to be considered. One of these could involve the manner in which the reducing solution is brought into contact with the glass fragments. Similar to what is done today for the restoration of large stained glass windows, instead of submerging the fragments in their totality in the reducing solution, a wet compress, soaked with the treating solution, could be used in order to produce the desired effect on the affected surface only. However, in this way, the solution may possibly not reach all the Mn in the alteration layer. Next to saturating the reducing solution with K, Na, and Ca ions, pH buffering might also help in limiting (part of) the glass damage.

The next steps in our study will involve attempts to decrease the undesired damage to the glass. In parallel, the efficiency with

which different reducing agents operate (such as citric acid, EDTA, acetylacetone) will be inter-compared. The possibility of performing laminography[41] instead of conventional tomography on intact (larger) samples will also be considered, since this would significantly reduce the stress and strain in the glass induced by sample preparation. Moreover, the production and weathering (*e.g.* by exposure to acids and $MnCl_2$ solutions) of glass fragments of controlled shape and composition will be tested, in order to obtain material equivalent to the historical glass samples used for the experiments described in this paper.

Acknowledgements

This research was supported by the Interuniversity Attraction Poles Programme—Belgian Science Policy (IUAP VI/16). The text also presents results of GOA "XANES meets ELNES" (Research Fund University of Antwerp, Belgium) and from FWO (Brussels, Belgium) projects no. G.0704.08 and G.01769.09. Special thanks to Ms Leonie Seliger, head of the stained-glass conservation studio (The Cathedral Studios—The Chapter of Canterbury Cathedral) for the supply of the archaeological samples. The authors gratefully acknowledge ESRF for granting beamtime (proposal EC-602).

Notes and references

1 O. Schalm, K. Proost, K. De Vis, S. Cagno, K. Janssens, F. Mees, P. Jacobs and J. Caen, *Archaeometry*, 2011, **53**(1), 103–122.
2 R. Newton and S. Davison, *Conservation of Glass*, Butterworth Heinemann, London, 1989.
3 E. V. Sayre, *Advances in Glass Technology*, 1963, Part 2, pp. 263–82.
4 M. K. Misra, K. W. Ragland and A. J. Baker, *Biomass Bioenergy*, 1963, **4**(2), 103–116.
5 W. B. Stern and Y. Gerber, *Archaeometry*, 2004, **46**(1), 137–156.
6 *The Pirotechnia of Vannoccio Biringuccio: the Classic Sixteenth-Century Treatise on Metals and Metallurgy*, ed. C. S. Smith and M. T. Gnudi, Dover, New York, 1990.
7 G. A. Cox and B. A. Ford, *J. Mater. Sci.*, 1993, **28**, 5637–5647.
8 A. Doménech-Carbó, M. T. Doménech-Carbó and L. Osete-Cortina, *Electroanalysis*, 2001, **13**(11), 927–935.
9 A. Silvestri, G. Molin and G. Salviulo, *J. Non-Cryst. Solids*, 2005, **351** (16–17), 1338–1349.
10 G. I. Cooper, G. A. Cox and R. Perutz, *J. Microsc.*, 1993, **170**(2), 111–118.
11 M. T. Doménech-Carbó, A. Doménech and L. Osete, *Microchim. Acta*, 2006, **154**, 123–142.
12 K. W. Mandernack, J. Post and B. M. Tebo, *Geochim. Cosmochim. Acta*, 1995, **59**(21), 4393–4408.
13 S. Fitz, *A New Method of Cleaning Browned Medieval Glass*, ICOM Committee for Conservation, 6th Triennial Meeting, Ottawa, 1981, pp. 1–6.
14 M. Torge, W. Müller, K. Adam and C. Köcher, Verbräunung von Gläsern durch Manganoxidation, in *2e Colloque du Programme Franco-Allemand de Recherche Pour la Conservation des Monuments Historiques*, Bonn, 1996, pp. 47–54.
15 L. Weber, Examination and Removal of Staining from Archaeological Glass, in *Diploma Thesis Submitted for the Degree of Konservierung und Restaurierung von Archäologischen, Ethnologischen und Kunsthandwerklichen Objekten*, Staatliche Akademie der Bildenden Künste, Stuttgart, 2005, pp. 86–88.
16 W. Müller, *Verbräunte mittelalterliche Glasmalereien*, ed. Leipzig, Verfahren zur Aufhellung, Leipzig, 2002, pp. 52–62.
17 R. Conradt, *J. Am. Ceram. Soc.*, 2008, **91**(3), 728–735.
18 B. C. Bunker, *J. Non-Cryst. Solids*, 1994, **179**, 300–308.
19 R. H. Doremus, *Earth Planet. Sci. Lett.*, 1998, **163**, 43–51.
20 J. Sterpenich and G. Libourel, *J. Non-Cryst. Solids*, 1998, **352**, 5446–5451.
21 H. Scholze, *J. Non-Cryst. Solids*, 1982, **52**, 91–103.
22 M. Schreiner, *Mikrochim. Acta*, 1991, **11**, 255–264.
23 M. Melcher and M. Schreiner, *Anal. Bioanal. Chem.*, 2004, **379**(4), 628–639.
24 M. Schreiner, G. Woisetschläger, I. Schmitz and M. Wadsak, *J. Anal. At. Spectrom.*, 1999, **14**(3), 395–403.
25 M. Melcher and M. Schreiner, *J. Non-Cryst. Solids*, 2006, **352**, 368–379.
26 G. Woisetschläger, M. Dutz, S. Paul and M. Schreiner, *Microchim. Acta*, 2000, **135**, 121–130.
27 B. Knight, in *Excavated Window Glass: a Neglected Source?*, ed. A. Roy and P. Smith, Preprints of the Contributions to the Copenhagen Congress, 1996, pp. 99–104.
28 C. Loisel, *Etude Sanitaire, Documentation et Analyses Physico-Chimiques, Vitraux XVIe siècle, Eglise Saint Julien, Luyères (10) Aube, Rapport no 1185A 30/09/2005*, Laboratoire de Recherche des Monuments Historiques, 2005, p. 12.
29 D. Hind, I. Marsden and C. Evans, *Archaeological Investigations at Sidney Sussex College*, Cambridge, 1994.
30 O. Schalm and K. Janssens, *Spectrochim. Acta, Part B*, 2003, **58**(4), 669–680.
31 B. Ravel and M. Newville, *J. Synchrotron Radiat.*, 2005, **12**, 537–541.
32 J. Susini, M. Salomè, B. Fayard, R. Ortega and B. Kaulich, *Surf. Rev. Lett.*, 2002, **9**, 203–211.
33 V. A. Solé, E. Papillon, M. Cotte, P. Walter and J. Susini, *Spectrochim. Acta, Part B*, 2007, **62**, 63–68.
34 O. Betz, U. Wegst, D. Weide, M. Heethoff, L. Helfen, W. K. Lee and P. Cloetens, *J. Microsc.*, 2007, **227**(Pt 1), 51–71.
35 A. C. Kak and M. Slaney, *Principles of Computerized Tomographic Imaging*, IEEE Press, 1988.
36 J. Radon, *Berichte Saechsische Akademie der Wissenschaften*, 1917, vol. 29, pp. 262–277.
37 J. Yi, A. M. Orville, J. M. Skinner, M. J. Skinner and G. B. Richter-Addo., *Biochemistry*, 2010, **49**(29), 5969–5971.
38 J. James-Smith, J. Cauzid, D. Testemale, L. Weihua, J. L. Hazemann, O. Proux, B. Etschmann, P. Philippot, D. Banks, P. Williams and J. Brugger, *Am. Mineral.*, 2010, **95**(7), 921–932.
39 E. Chalmin, C. Vignaud, H. Salomon, F. Farges, J. Susini and M. Menu, *Appl. Phys. A: Mater. Sci. Process.*, 2006, **83**, 213–218.
40 E. Chalmin, F. Farges and G. E. Brown, *Contrib. Mineral. Petrol.*, 2009, **157**, 111–126.
41 K. Krug, L. Porra, P. Coan, A. Wallert, J. Dik, A. Coerdt, A. Bravin, M. Elyyan, P. Reischig, L. Helfen and T. Baumbach, *J. Synchrotron Radiat.*, 2008, **15**(1), 55–61.

